J Appl Electrochem (2008) 38:1195–1201
DOI 10.1007/s10800-008-9537-z

ORIGINAL PAPER

Durability of carbon-supported manganese oxide nanoparticles for the oxygen reduction reaction (ORR) in alkaline medium

I. Roche · E. Chaînet · M. Chatenet · J. Vondrák

Received: 14 September 2007 / Revised: 25 February 2008 / Accepted: 25 February 2008 / Published online: 8 March 2008

Abstract MnO_x/C-based electrocatalysts, prepared by the chemical deposition of manganese oxide nanoparticles on carbon, were tested towards the Oxygen Reduction Reaction (ORR) in their as-synthesized state and after ageing, either in ambient air for a year (mild ageing) or in an O_2-saturated molar KOH solution at 80 °C for three weeks (premature ageing). For each electrocatalyst, the morphology and composition were characterised using TEM, XRD and chemical analysis. ORR kinetic parameters were evaluated using the Rotating Disk Electrode (RDE) and Rotating Ring Disk Electrode (RRDE) setups. Whilst the oxygen reduction activity of the electrocatalysts barely changes after mild ageing, it decreases after premature ageing following dramatic modifications to both the chemical and crystalline structures of the carbon-supported MnO_x nanoparticles. The peroxide yield also sharply increases after premature ageing. Doping MnO_x/C with nickel or magnesium divalent cations is beneficial since it improves both the catalytic activity and selectivity towards the 4-electron ORR pathway, even after ageing.

I. Roche · E. Chaînet · M. Chatenet
Laboratoire d'Electrochimie et de Physicochimie des Matériaux et des Interfaces, LEPMI-ENSEEG, UMR 5631 CNRS-INPG-UJF, BP 75, 38402 Saint Martin d'Heres Cedex, France

I. Roche (✉)
Fuel Cell Research Laboratory, School of Chemical Engineering and Advanced Materials, Merz Court, Newcastle University, Newcastle upon Tyne NE1 7RU, UK
e-mail: Ivan.Roche@newcastle.ac.uk

J. Vondrák
Institute of Inorganic Chemistry, Academy of Sciences of the Czech Republic, Rez, 250 68 Prague, Czech Republic

Keywords Oxygen reduction reaction · Rotating ring-disc electrode · Carbon-supported manganese oxide · Nickel doping · Durability

1 Introduction

The air electrode is a key component of Alkaline Fuel Cell (AFC) systems. One great advantage of the alkaline medium is that platinum, known to be the best electrocatalyst for the Oxygen Reduction Reaction (ORR) [1], can efficiently be replaced by less expensive oxygen reduction catalysts in the AFC cathode, without detrimental impact on performance. To this end, great attention has been devoted to the formulation of *activated* carbon powders, carbon-supported mixed oxides and macrocycles [2] or other platinum-free electrocatalysts based on Co, Ru, Sn and Ni [3]. Today, one of the most popular alternatives to the benchmark carbon-supported platinum electrocatalyst is Ag/C [4–9], due to its rather high ORR activity and reasonable cost. Our group and several others have recently shown that manganese oxides dispersed onto carbon powder with a high surface area are also promising ORR electrocatalysts, displaying high activity and being of low cost [10–17]. The ORR mechanism on unsupported micro-sized MnO_x particles, synthesized using techniques other than those referenced herein, was described [18] as a dual pathway, consisting of competition between the 4-electron mechanism with a partial reduction with 2 electrons yielding hydrogen peroxide ions (HO_2^-), followed by either a 2-electron reduction or a disproponation reaction of HO_2^- in solution. However, our nickel- or magnesium-doped carbon-supported MnO_x nanoparticles favour the 4-electron pathway, whilst exhibiting remarkable catalytic

oxygen reduction activity [19]. Such features render them very attractive electrocatalysts for the air-cathode of an AFC, provided their catalytic durability is sufficient, which has not yet been evaluated.

The aim of the present paper is to complement our previous work [16, 19], and to study the influence of ageing on MnO_x/C electrocatalysts in terms of (i) carbon-supported particle morphology, (ii) ORR activity and (iii) ORR pathway (peroxide yield).

2 Experimental

2.1 Ageing of the MnO_x/C electrocatalysts

Three different electrocatalysts were considered in the present work: MnO_x/C, Ni–MnO_x/C and Mg–MnO_x/C [16, 19]. Their deposition onto Chezacarb SH (Chemopetrol, Litvinov) carbon black (specific area close to 1,000 $m^2\ g^{-1}$) was described in reference [12]. We characterised the physicochemical and electrochemical properties of the electrocatalysts in their as-synthesized state and after *mild* or *premature* ageing. The *mild* ageing consisted of 1 year storage in ambient air; it mimics shelf storage between synthesis and the first use of the electrode in the AFC. The *premature* ageing was carried out as follows: 150 mg of each MnO_x/C powder was introduced into a cell containing 50 mL of molar potassium hydroxide solution (Normapur, PROLABO) saturated with oxygen by permanent O_2 bubbling and maintained at a constant temperature 80 (±1) °C at open circuit potential (ocp). Such ageing at ocp is very severe, as previously shown for platinum-containing electrocatalysts [20], and so can be considered as an accelerated ageing procedure. Each powder was recovered by decantation/filtration. The prematurely aged powders were washed three times with pure water and gently dried in air at 50 °C prior to subsequent characterisations.

In the following text, mildly aged materials are noted as $MnO_x/C^{\#}$ or Me–$MnO_x/C^{\#}$ (Me = Ni or Mg), whilst prematurely aged powders are noted as MnO_x/C* or Me–MnO_x/C*.

2.2 Physicochemical characterisations of the carbon-supported MnO_x nanoparticles

The various MnO_x/C powders were characterised using Transmission Electron Microscopy (TEM, Jeol 2011). X-ray Diffraction (XRD) patterns were also obtained for all the materials, using a Philips TW 1730 vertical goniometer/diffractometer equipped with a diffracted-beam monochromator using Fe(K_α) radiation and recalculated for Cu(K_α) radiation. Chemical analyses were performed by the *service central d'analyse* (CNRS, Vernaison, France). The amount of water in the samples was evaluated by Thermo Gravimetric Analysis (TGA) performed on a Netsch STA409 PC apparatus, under 80 mL min^{-1} nitrogen flow.

2.3 Electrochemical setups

Rotating Disk Electrode (RDE) measurements were performed in an O_2-saturated 1 mol L^{-1} KOH solution at 25 (±1) °C in a four electrode Pyrex cell to evaluate ORR kinetic parameters (Specific and Mass Activities, SA and MA) of all our materials using the electrochemical setup previously described [19]. Rotating Ring Disk Electrode (RRDE) experiments were carried out [19] in O_2-saturated 0.1 mol L^{-1} KOH solution at 25 (±1) °C to estimate the percentage of peroxides formed per molecule of reduced oxygen as a function of potential. Each active layer was deposited from a 10 μL (RDE) or 20 μL (RRDE) drop of ink containing 25 mg of MnO_x/C, Ni–MnO_x/C, Mg–MnO_x/C or raw carbon black, 1 mL of water, 0.6 mL of ethanol and 3 μL of PTFE beads in solution (60 wt.%, Dupont) [9, 16, 19].

Chronoamperograms were also recorded on the active layers in O_2-saturated molar KOH solution at 25 (±1) °C for a RDE speed of rotation of 500 rpm in a three electrode cell using a computer-controlled potentiostat (Solartron SI 1287). The potential was kept at 0 V vs. NHE (see Sect. 3.1). The ORR current variation was measured for approximately 200 h for each electrocatalyst.

3 Results and discussion

3.1 In situ ageing during ORR at imposed potential

At 0 V vs. NHE, which mimics the operating potential of an AFC cathode, MnO_2 starts to be reduced into manganite (MnOOH) [13, 16]. Figure 1a shows examples of chronoamperograms for MnO_x/C and Ni–MnO_x/C. The initial potentials are close to those measured in the quasi-steady state voltammetries under the same conditions at 0 V vs. NHE [19]. The oxygen reduction currents decrease substantially within the first 10 h, after which time the decline is slower. The initial rapid loss of activity may result from capacitive effects: (i) double layer charge/discharge in the first few seconds and (ii) proton insertion in the following minutes, the so-called fly-wheel effect [15]. By contrast, the *long-term* (slow) losses are faradaic, and could be linked to a decrease in specific area or the loss of active materials. Figure 1b shows the corresponding $\log |i| = f(t)$ representations for MnO_x/C and Ni–MnO_x/C. The $\partial \log |i| / \partial t$ slopes are ca. −0.023 and −0.001 (dec. h^{-1}) for MnO_x/C

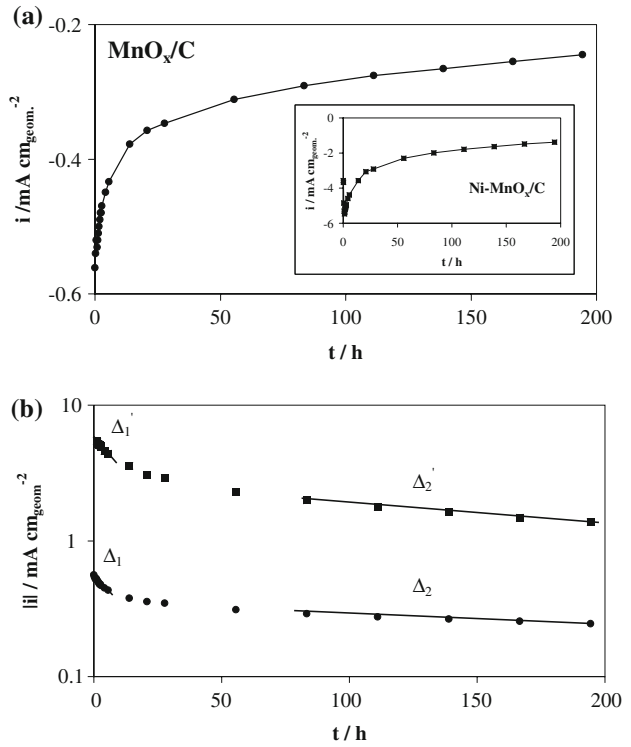

Fig. 1 (**a**) ORR chronoamperometries (E = 0 V vs. NHE) measured on MnO_x/C (rounds) and Ni–MnO_x/C (squares) in O_2-saturated molar KOH solution at 25 °C, geometrical area = 0.196 cm^2. (**b**) Corresponding log |i| = f(t) curves. Δ_i and Δ_i' are the ∂log |i|/∂t (dec. h^{-1}) slopes respectively for MnO_x/C (rounds) and Ni–MnO_x/C (squares). Δ_i ca. −0.023 and −0.001 mA $cm_{geom.}^{-2}$ h^{-1} compare Δ_i' ca. −0.024 and −0.001 mA $cm_{geom.}^{-2}$ h^{-1}

compare ca. −0.024 and −0.001 (dec. h^{-1}) for Ni–MnO_x/C. As the slopes are rather similar, the mechanisms of the fast (up to 10 h) and long term (in excess of 80 h) loss of activity could be the same for the doped and undoped MnO_x/C-based catalysts. To more fully understand the loss of ORR activity over time, we evaluated the impact of ageing on (i) the morphology and chemistry of the MnO_x/C electrocatalysts (see Sect. 3.2) and (ii) ORR activity and pathway (see parts 3.3 and 3.4).

3.2 Physicochemical characterisations of the MnO_x/C electrocatalysts

3.2.1 Metal loading and oxygen/water content determinations

The results of chemical analyses of the three $MnO_x/C^{\#}$ [19] and MnO_x/C^* electrocatalysts are presented in Table 1, along with their water loadings (evaluated by TGA, Fig. 2). Table 1 also presents the analyses relative to the raw carbon black Chezacarb SH. Although the oxygen loadings could not be measured experimentally, they can be estimated assuming that, except C, Mn, Ni, Mg, H, K and Si or impurities (<1 wt.%), the only species are oxygen. The presence of O was first linked to that of Mn, Ni or Mg oxides, water [19], and carbon surface oxides (e.g. quinones, carboxylic acids, etc. [24]). Second, we assumed that (i) all Mn and Me are present as MnO_2 and $Me(OH)_2$, and (ii) the oxygen content on the carbon surface is 100 wt.% minus the wt.% of all the other elements (Table 2).

The as-synthesized MnO_x/C-based electrocatalysts exhibited a [Mn/(C + Mn + O + Me)] loading of around 20 wt.% [12, 15]. These loadings decreased slightly after *mild* ageing (Table 1), probably reflecting, first, water uptake and, second, an increase in the overall oxygen content, certainly due to the surface oxidation (acidic groups [24]) of the high specific area carbon black more than a loss of active material.

Under *premature* ageing, being given that for all our MnO_x/C-based materials (i) some active material, Mn, Ni and Mg, is lost (the C/Mn and C/Me ratios increase), (ii) the Mn loadings decrease with rather constant weight ratio (2.7), and (iii) the Mn/Me weight ratios remain identical (Mn/Ni ∼ 2 and Mn/Mg ∼ 9), the carbon-supported MnO_x nanoparticles are thus homogeneously attacked by the alkaline solution. Indeed, manganite (Mn^{III}) is soluble in alkaline solution, whereas carbon should be immune [21], since no HO_2^- is produced at open circuit potential (E > +0.1 V vs. NHE). Si and Na wt.% increase (Table 1)

Table 1 Chemical analysis of the as-synthesized MnO_x/C materials upon synthesis (after *mild* (#) and *premature* (*) ageing

Catalysts	C (wt.%)	Mn (wt.%)	Me (wt.%)	H_2O (wt.%)	Na (wt.%)	K (wt.%)	H (wt.%)	Si (wt.%)
$MnO_x/C^{\#}$	22	14	–	∼50	$<5 \times 10^{-2}$	3	3	<0.1
Ni-$MnO_x/C^{\#}$	20	11	5	∼40	$<5 \times 10^{-2}$	1	2	<0.1
Mg-$MnO_x/C^{\#}$	38	20	2	∼20	$<5 \times 10^{-2}$	2	2	<0.2
MnO_x/C^*	15	6	–	∼17	1	27	1	4
Ni–MnO_x/C^*	14	5	2	∼12	1	24	1	6
Mg–MnO_x/C^*	13	9	1	∼9	1	19	1	9
Carbon	92	–	–	–	$<5 \times 10^{-2}$	$<5 \times 10^{-2}$	1	<0.1

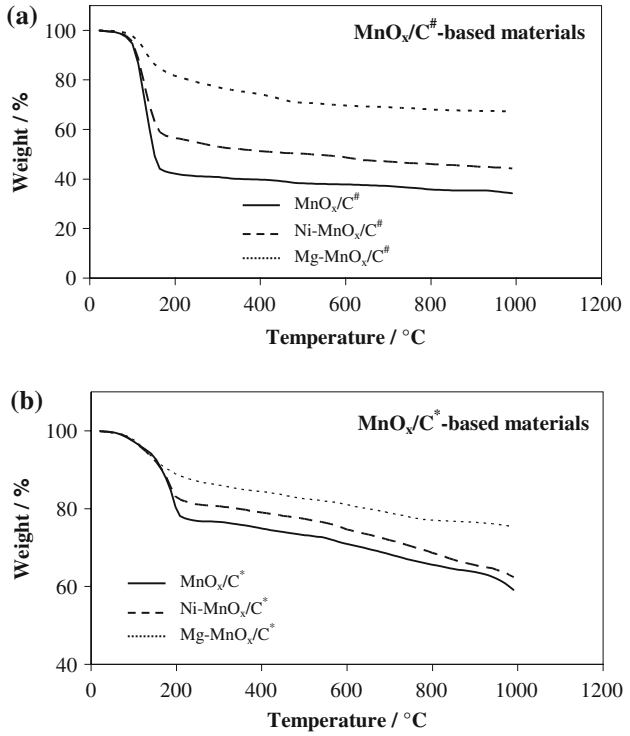

Fig. 2 (**a**) TGA plots for the $MnO_x/C^{\#}$-based materials between 25 and 1,000 °C. (**b**) TGA curves for the MnO_x/C^*-based materials between 25 and 1,000 °C

Table 2 The weight of oxygen present in MnO_2, $Me(OH)_2$ (Me = Ni, Mg) and H_2O are estimated starting from the loadings of Mn, Me and H_2O, respectively (Table 1)

Catalysts	O_{MnO_2} (wt.%)	$O_{Me(OH)_2}$ (wt.%)	O_{H_2O} (wt.%)	O_{carbon} (wt.%)
$MnO_x/C^{\#}$	8	–	44	5
Ni–$MnO_x/C^{\#}$	6	3	36	17
Mg–$MnO_x/C^{\#}$	12	3	18	4
MnO_x/C^*	3	–	15	33
Ni–MnO_x/C^*	3	1	11	40
Mg–MnO_x/C^*	5	1	8	43

The amount of oxygen contained in the carbon surface oxide is 100 wt.% minus the wt.% of all the other elements

may follow the Pyrex cell (80 at.% Si, few at.% Na) corrosion in the strong alkaline solution. Resulting Na^+ species, as well the Na^+ ions contained in Normapur® KOH (0.5 wt.% according to PROLABO), could likely enter the MnO_x lattice [22]. Although no studies were done on the potential for Si-doping of the MnO_x lattice, we believe that the adsorption of Si-containing species (like SiO_2) over our materials could explain the increasing Si contents.

The water loadings (determined by TGA, Fig. 2) are ca. 50, 40 and 20 wt.% for $MnO_x/C^{\#}$, Ni– and Mg–$MnO_x/C^{\#}$, respectively, compare ca. 17, 12 and 9 wt.% for MnO_x/C^*, Ni– and Mg–MnO_x/C^* (Table 1). Our results show mainly physically adsorbed water (temperature range 100–200 °C [23]) in our $MnO_x/C^{\#}$ materials. Undoped $MnO_x/C^{\#}$ displays an additional shoulder at ca. 450 °C (Fig. 2a), which is not observed in the doped materials, following MnO_x crystalline modifications due to (i) the insertion of divalent ions into the lattice and/or (ii) to variation in the amount of chemically bonded water, which depends on the MnO_2 phase [24]. Finally, the high hydration of the $MnO_x/C^{\#}$ materials probably results from water filling of the carbon microporosity by capillary condensation. All the MnO_x/C^*-based materials exhibit the same TGA profiles (Fig. 2b), indicating that their structures no longer differ sharply in terms of chemically-bonded water (temperature range 200–400 °C [23]). Also, the overall weight loss is ca. 15–30% smaller than the $MnO_x/C^{\#}$ materials, probably reflecting a decrease in the carbon microporosity under such severe conditions (as previously noted by Chatenet et al. for carbon-supported platinum nanoparticles [25]).

The loadings corresponding to oxygen in carbon surface oxide groups (excluding from MnO_2, $Me(OH)_2$ and H_2O) are estimated to be ca. 5, 17 and 4 wt.% for $MnO_x/C^{\#}$, Ni– and Mg–$MnO_x/C^{\#}$ respectively, compare ca. 33, 40 and 43 wt.% for the corresponding MnO_x/C^* materials (Table 2). The rather similar loadings of oxygen after *premature* ageing could result from an equilibrium between the carbon surface and the oxygen-saturated KOH medium, reflecting (i) the stabilisation of the number of oxygenated groups (and water) on the carbon surface during the *premature* ageing, and (ii) the great dependence of the oxygen coverage of the MnO_x/C^* catalysts on the ageing conditions, and less so on the nature of the MnO_x phase. The carbon black Chezacarb presents many graphitized areas [19], supposedly resistant to (electro)chemical oxidation (already shown for PA [26] and PEM [27] Fuel Cells). Such high oxidation of our materials would reflect the oxidation of benzene-like cycles on the carbon surface during the premature ageing.

To summarize, knowing that (i) the Chezacarb initially is resistant to such a severe ageing, (ii) our materials contain substantial amounts of Mn^{III} (which confers good ORR activity [19] but is prone to dissolution in alkaline medium [21]) and (iii) the K, Na or Si loadings do not increase as much as the metal loadings decrease, our elemental analyzes undoubtedly show that some active material (MnO_x or Me–MnO_x) is dissolved during *premature* ageing, implicating the decrease in ORR activity (Fig. 1).

3.2.2 *TEM and XRD characterisations*

The morphology of the as-synthesized MnO_x nanoparticles dispersed over the carbon black Chezacarb has been previously studied [19]. No significant differences in particle

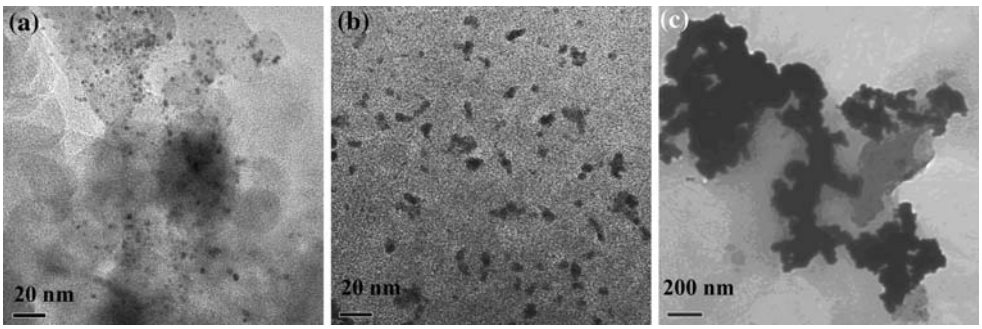

Fig. 3 (**a**) TEM images of $MnO_x/C^{\#}$ after *mild* ageing. (**b**, **c**) TEM images of MnO_x/C^* after *premature* ageing

morphology are detected (either from TEM or XRD) for MnO_x/C and $MnO_x/C^{\#}$ materials. An sample TEM image is presented in Fig. 3a. Again, there is strong evidence that *mild* ageing barely affects the MnO_x/C electrocatalysts.

Figure 3b and c show examples of TEM images for the prematurely aged MnO_x/C^*. The MnO_x particles are no longer spherical and are rather heterogeneously dispersed over the carbon. Moreover, agglomerates and large particles of a few 10 nm have formed upon *premature* ageing. The XRD pattern for MnO_x/C^* shows the presence of manganese carbonate species, such as $H_3Mn_3(CO)_{12}$, while γ-MnO_2 (predominant in the as-synthesized materials) is a minor component. The average particle diameter has substantially increased to ca. 57 nm. The particle ageing process is complex. On the one hand, mono-crystalline particles are observed (Fig. 3b): these can result from either spillover of metal (Mn, Ni or Mg) atoms from *corroding* nanoparticles to *building* nanoparticles (2D-Ostwald ripening, as shown in the case of platinum) [28, 29], or from the dissolution of a *small* nanoparticle followed by the diffusion of the metal cations in solution and their redeposition on another, larger, nanoparticle (3D-Oswald ripening). On the other hand, large agglomerates of polycrystalline nanoparticles are also detected by TEM (Fig. 3c); these are likely formed by nanoparticles spilling over the carbon surface or carbon corrosion yielding unsupported MnO_x nanoparticles, followed by their aggregation to particles that remain anchored. However, as (i) we did not detect unsupported MnO_x particles and (ii) carbon should be rather stable in the present case (see above), the carbon bulk corrosion scenario does not appear very likely (even if surface oxidation occurs, as shown in Sect. 3.2.1). The observations are similar for the doped materials. Starting from the XRD patterns, average diameters of ca. 37 and 51 nm were calculated for Ni- and Mg–MnO_x/C^*, respectively (Table 3). As for the undoped MnO_x/C^*, *premature* ageing changed the chemical and crystalline structures of the doped MnO_x particles, indicating that the stabilization obtained by doping as reported in the literature [16, 19] is not efficient under such severe ageing conditions. In particular, doping does not prevent the reduction of manganese dioxide into MnOOH species and its subsequent dissolution.

Table 3 Diameters calculated from XRD patterns after *mild* ($^{\#}$) or *premature* (*) ageing

Catalysts	d (nm)	MA (A g^{-1})	SA (μA cm^{-2})	b (V dec^{-1})
$MnO_x/C^{\#}$	4	11.0	3.9	−0.062
Ni–$MnO_x/C^{\#}$	6	36.9	18.6	−0.059
Mg–$MnO_x/C^{\#}$	6	25.9	13.4	−0.044
MnO_x/C^*	57	6.2	30.5	−0.098
Ni–MnO_x/C^*	37	14.0	43.8	−0.074
Mg–MnO_x/C^*	51	5.1	21.7	−0.074
10 wt.% Pt/Vulcan XC72	2	40.1	25.8	−0.081

ORR Tafel slopes, Mass activities (MA) measured at 0 V vs. NHE and corresponding specific activities (SA) in O_2-saturated 1 M KOH solution at 25 °C

3.3 Electrochemical stability and ORR activity of MnO_x/C-based electrocatalysts

Cyclic voltammetry in deaerated molar potassium hydroxide revealed the stability of doped-MnO_x/C [16, 19]. For all the MnO_x/C^*-based electrocatalysts, *premature* ageing decreased both the proton insertion/de-insertion capacity (ca. 90%) and the double-layer response (see the example of MnO_x/C^* and Ni–MnO_x/C^*, Fig. 4 compare Fig. 1 in reference [16] for comparison). This is consistent with (i) the MnO_x particle agglomeration monitored by TEM, (ii) the mean diameter increase monitored by XRD and (iii) the decrease of active material content (see Sect. 3.2).

We evaluated the ORR activity of the MnO_x/C-based active layers in oxygen-saturated molar KOH solution at 25 °C. The current densities (i_k) were corrected for oxygen diffusion both in the solution and the active layer [19], the pure faradaic current under O_2 being obtained following subtraction from the *blank* current under argon under the same sweep conditions [19]. Change in the ORR activity is almost negligible after *mild* ageing, following the relatively

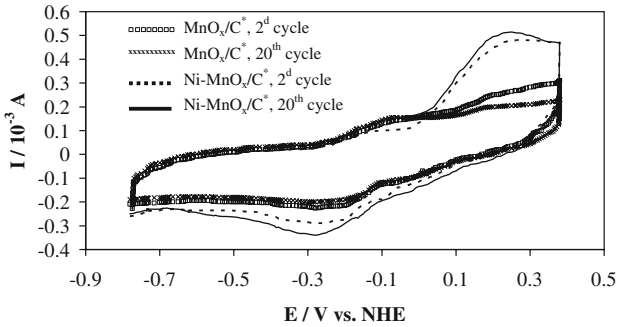

Fig. 4 2[d] and 20th cyclic voltammogram cycles in argon-saturated 1 M KOH at 25 °C for MnO_x/C^* and Ni–MnO_x/C^*, geometrical area = 0.196 cm^2, sweep rate 0.1 V s^{-1}

unchanged morphology and chemistry of the $MnO_x/C^{\#}$ materials (see Sect. 3.2).

In contrast, the prematurely aged materials display mass activities which are much smaller compared to the as-synthesized materials. With respect to the ORR kinetic parameters, the mass activities at 0 V vs. NHE for the undoped MnO_x/C are ca. 11 and 6 A g^{-1} (Table 3) before and after severe ageing. The weak electrocatalytic activity of the MnO_x/C^* (see above) is susceptible to premature ageing as the first step for ORR is proton insertion into the MnO_x lattice [19]. Moreover, the ORR MA decrease is balanced by the decrease in active material (MnO_x) content in the electrocatalyst after severe ageing (Table 1). In addition, the Me–MnO_x/C are susceptible to loss of kinetic activity with severe ageing, their MA decreasing from ca. 37 and 26 A g^{-1} for Ni– and Mg–$MnO_x/C^{\#}$ to ca. 14 and 5 A g^{-1} at 0 V vs. NHE for Ni– and Mg–MnO_x/C^*. Nevertheless, it appears that nickel or magnesium doping remains beneficial with regard to the ORR kinetics, even after *premature* ageing, Ni doping being the most interesting in term of ORR activity. The specific activities (SA) of MnO_x/C^* are higher (Table 3), following dramatic changes in the chemistry and morphology of MnO_x nanoparticles, due to severe ageing. As MnO_2 is a minor component in aged samples (see Sect. 3.2.2) the presence of this phase is not necessary for good ORR activity. MA values are calculated from the effective MnO_2 loading (see [19]) for the prematurely aged materials (Table 1), which is then an approximation since the MnO_x/C^*-based materials display altered chemical and crystalline structures of MnO_x particles (see Sect. 3.2). In the same way, the specific activities (SA) of the prematurely aged materials, calculated starting from the MA and XRD diameter values and considering the MnO_2 particles, are not strictly comparable to those of MnO_x/C [19].

Finally, *premature* ageing is more dramatic than in situ ageing at imposed ORR potential (see Sect. 3.1), following conclusions on carbon-supported platinum nanoparticles [20]. This is mainly due to (i) higher temperature (80 compare 25 °C) yielding faster corrosion/dissolution or particle agglomeration kinetics, and (ii) more anodic potential (ocp) for the *premature* ageing.

3.4 Evolution of the ORR pathway for the aged materials

RRDE experiments were undertaken in order to evaluate the ORR pathway for aged MnO_x/C electrocatalysts. The overall number of electrons (n_t) per oxygen molecule reduced on the RRDE disk was determined in the low current density range, in O_2-saturated KOH solution at 25 °C for a speed of rotation of 500 rpm [19]. The electronic (x^e) and molar (x^m) proportions of hydrogen peroxide ions formed per reduced oxygen molecule were determined [30], in the low current densities range, before [19] and after *premature* ageing. Figure 5 shows that for all the electrocatalysts, *premature* ageing modifies the ORR mechanism: the 2-electron pathway, yielding HO_2^- ions, becomes predominant. For example, at $E_D = 0$ V vs. NHE, the experimental x^m values are ca. 23, 12 and 5% for MnO_x/C, Mg– and Ni–MnO_x/C [19], respectively, compare ca. 64, 60 and 54% for the corresponding MnO_x/C^*-based electrocatalysts (Table 4). The increase in hydrogen peroxide yield at this potential could result from (i) morphological/chemical changes in the manganese oxide nanoparticles and/or (ii) severe loss of active material (MnO_x, or Me–MnO_x), yielding a higher apparent carbon area (carbon quantitatively producing hydrogen peroxide) [1, 31]. However, the benefits of doping are not completely lost with *premature* ageing: it still contributes to partially direct the ORR mechanism towards the 4 electrons pathway, yielding less hydrogen peroxide ions than undoped MnO_x/C^*. A lower peroxide yield for Me–MnO_x/C is interesting with regard to the faradaic efficiency or the durability of the cathode electrocatalyst.

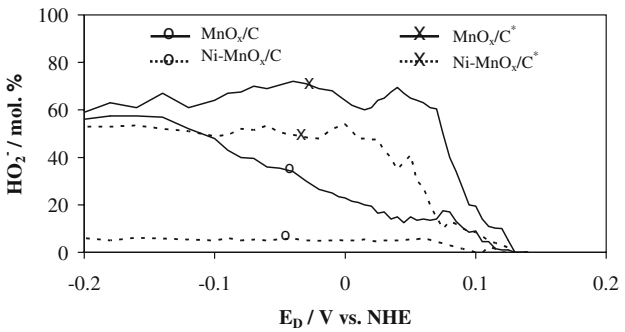

Fig. 5 Molar proportions of HO_2^- ions formed on the RRDE disc per reduced O_2 mole, MnO_x/C^*, Ni–MnO_x/C^*, MnO_x/C and Ni–MnO_x/C as a function of E_D; O_2-saturated 0.1 M KOH solution at 25 °C, E_R = +0.45 V vs. NHE, 500 rpm

Table 4 Number of electrons n_t exchanged per reduce O_2 molecule on the disc and corresponding electronic x^e and molar x^m proportions of HO_2^- formed on the disc at $E_D = 0$ V vs. NHE

Catalysts	n_t	x^e (%)	x^m (%)
MnO_x/C*	2.7	48	64
Mg–MnO_x/C*	2.8	39	60
Ni–MnO_x/C*	2.9	37	54

O_2-saturated 0.1 M KOH solution at 25 °C, E_R = +0.45 V vs. NHE, 500 rpm

4 Concluding comments

The MnO_x/C-based electrocatalysts do not suffer drastic ageing in ambient air: upon such mild ageing, the MnO_x nanoparticles keep similar crystalline and chemical structures. Their electrochemical activities remain comparable to those of the as-synthesized electrocatalysts.

By contrast, *premature* ageing yields important changes in MnO_x particles dispersed onto the carbon in term of their crystalline and chemical structures. The prematurely aged nanoparticles contain high amounts of manganese carbonates and their sizes significantly increase to a few 10 nm. In addition their dispersion over the carbon surface is no longer homogeneous. Upon *premature* ageing, the manganese mass loading loss and the sharp increase in particle size are mainly responsible for the strong loss of ORR mass-activity of the MnO_x/C* electrocatalysts. Conversely, the intrinsic ORR activity is barely affected by premature ageing: the specific activities being comparable after premature ageing. Moreover, the prematurely aged Me–MnO_x/C* catalysts still exhibit a greater ORR activity than the undoped MnO_x/C*. While the beneficial effect of Mg or Ni-doping remains evident with respect to the ORR kinetics after premature ageing, the ORR mechanism on the MnO_x/C*-based electrocatalysts is greatly affected: the proportion of hydrogen peroxide formed per reduced O_2 increases significantly, even if the Me-doping still contributes to limit the HO_2^- yield. The ORR mechanism being directed more towards the 2-electron pathway, it could be detrimental to the overall stability of the air-cathode. The latter could be responsible for the decreased manganese loadings and the chemical/structural changes of the MnO_x particles, as well as favour their rapid ageing.

Acknowledgments This project was supported by the Grant Agency of the Czech Republic (project N° 104/02/0731), by the Grant Agency of Academy of Sciences (N° 403/002 and KJB 481 3302) and by the Ministry of Education of the Czech Republic (Project N° MSM 262200010). It was also supported by the Ministry of Education and Research of France (Project N° PF 2002 88 2) and by the CNRS (Project N° 18105).

References

1. Kinoshita K (1992) In: Wiley (ed) Electrochemical oxygen technology. New York
2. Lamminen J, Kivisaari J, Lampinen MJ, Viitanen M, Vuorisalo J (1991) J Electrochem Soc 138:905
3. Chang CC, Wen TC (1997) Mater Chem Phys 47:203
4. Geniès L (1999) Thèse de doctorat. INPG
5. Illiev I, Mrha J, Kaisheva A, Gamburzev S (1976) J Power Sources 1:35
6. Furuya N, Ichinose O, Uchimura A (1997) ISE meeting, Paris, abstract 611
7. Zoval JV, Stiger RM, Biernacki PR, Penner RM (1996) J Phys Chem 100:837
8. Zoval JV, Biernacki PR, Penner RM (1996) Anal Chem 68:1585
9. Chatenet M, Geniès-Bultel L, Aurousseau M, Durand R, Andolfatto F (2002) J Appl Electrochem 32:1131
10. Zoltowski P, Drazic DM, Vorkapic L (1973) J Appl Electrochem 3:271
11. Vondrák J, Sedlaříková M, Novák V (1998) J New Mater Electrochem Syst 1:25
12. Bezdička P, Grygar T, Klápště B, Vondrák J (1999) Electrochim Acta 45:913
13. Klápště B, Vondrák J, Velická J (2002) Electrochim Acta 47:2365
14. Vondrák J, Klápště B, Velická J, Sedlaříková M, Černý R (2003) J Solid State Electrochem 8:44
15. Vondrák J, Klápště B, Velická J, Sedlaříková M, Novák V, Reiter J (2005) J New Mater Electrochem Syst 8:1
16. Vondrák J, Klápště B, Velická J, Sedlaříková M, Reiter J, Roche I, Chainet E, Fauvarque JF, Chatenet M (2005) J New Mater Electrochem Syst 8:209
17. Ticianelli EA, Lima F, Calegaro M (2006) 209th ECS spring meeting, Denver, abstract 301
18. Mao L, Zhang D, Sotomura T, Nakatsu K, Koshiba N, Ohsaka T (2003) Electrochim Acta 48:1015
19. Roche I, Chainet E, Chatenet M, Vondrák J (2007) J Phys Chem C 111:1434
20. Chatenet M, Aurousseau M, Durand R, Andolfatto F (2003) J Electrochem Soc 150:D47
21. Pourbaix M (1963) In: Gauthier-Villard (ed) Atlas d'équilibres électrochimiques. Paris
22. Sauvage F, Baudrin E, Tarascon JM (2007) Sens Actuators B 120:638
23. Kanungo SB (1979) J Catal 58:419
24. Anderson TN (1996) In: Bockris JOM et al. (eds) Modern aspects of electrochemistry, vol 30, Chapter 4. Plenum Press, New York
25. Chatenet M (2000) Thèse de doctorat. INPG
26. Kinoshita K, Bett J (1973) Carbon 11:237
27. Stevens DA, Dahn JR (2005) Carbon 43:179
28. Akira T, Taniguchi A, Maekawa J, Siroma Z, Tanaka K, Kohyama M, Yasuda K (2006) J Power Sources 159:461
29. Ferreira PJ, O' GJL, Shai-Horn Y, Morgan D, Makharia R, Kocha S, Gasteiger HA (2005) J Electrochem Soc 152:A2256
30. Albery WJ, Hitchman ML (1971) In: Ring-disk electrodes. Oxford University Press, Oxford, pp 17–28
31. Geniès L, Faure R, Durand R (1998) Electrochim Acta 44:1317